Clays and Clay Minerals, Vol. 63, No. 6, 414–431, 2015.

MINERALOGICAL EVOLUTION OF DI- AND TRIOCTAHEDRAL SMECTITES IN HIGHLY ALKALINE ENVIRONMENTS

KERSTIN ELERT*, EDUARDO SEBASTIÁN PARDO, AND CARLOS RODRIGUEZ-NAVARRO
Department of Mineralogy and Petrology, University of Granada, Fuentenueva S/N, 18002 Granada, Spain

Abstract—The mineralogical evolution of di- and trioctahedral smectites (*i.e.* montmorillonite and saponite) exposed to high-pH environments has been studied to determine the influence of compositional differences on clay dissolution and the formation of new phases. The present study helps to gauge the effects of highly alkaline solutions on the swelling capacity of smectitic clays and experimental results are extrapolated to predict the behavior of smectite-rich soils in various technical applications such as nuclear-waste storage and architectural conservation. The present study revealed extensive dissolution of montmorillonite in 5 M NaOH or 5 M KOH solutions and the neoformation of various zeolites, thereby reducing the clay's swelling capacity significantly. Saponite, in contrast, experienced less pronounced changes, including transformation into a randomly interstratified saponite-chlorite and a Si-rich amorphous phase. These changes only provoked a partial reduction in swelling capacity. The results imply that under repository conditions (*e.g.* alkaline environment caused by hyperalkaline fluids released during concrete leaching), the slow and limited transformation of saponite into corrensite-type minerals would be beneficial for preserving the clay's swelling capacity and, therefore, its effectiveness as a sealing material. Conversely, the loss of swelling capacity as a result of zeolite formation in montmorillonite observed in the present experiments would limit the clay's effectiveness as a sealing material in waste repositories. In the case of earthen architecture conservation, alkaline consolidation treatments aimed at reducing the soils' swelling capacity and, thereby, improving water resistance, would only be effective for treating earthen structures made of soils rich in dioctahedral smectites. Soils containing trioctahedral smectites, in contrast, are not likely to improve their water resistance because the swelling capacity will only be partially reduced.

Key Words—Alkaline Treatment, Clay Swelling, Earthen Architecture Consolidation, Montmorillonite, Saponite, Zeolites.

INTRODUCTION

The reactivity of smectitic clays in high-pH environments has been investigated extensively in recent years as a result of their use as sealing materials in nuclear and hazardous-waste repositories (Gaucher and Blanc, 2006, and references therein). Their low permeability and high plasticity, swelling, buffering, and ion-exchange capacity make smectites ideal candidates for use as sealing materials (Villar *et al.*, 2006). Under repository conditions, high-pH environments are created by hyperalkaline fluids (pH $\approx$ 13) released by concrete used for structural support. The reactivity of these clay minerals under highly alkaline conditions is, thus, of special importance to predict their effective service life and to prevent hazardous leak events.

The reactivity of smectitic clays exposed to highly alkaline solutions is also of relevance in the consolidation of earthen structures made of adobe or rammed earth, one of the greatest challenges in architectural conservation (Elert *et al.*, 2015). Conventional consolidation treatments (*e.g.* application of synthetic polymers or alkoxysilanes) often only aim at diminishing the alteration effects by increasing mechanical strength and do not tackle the cause of the problem. Over time, the consolidation effect is lost because the process that causes the damage to the earthen material, that is, the swelling and contraction of clay minerals exposed to humidity, especially severe in the case of smectites, continues (Doehne and Price, 2010). The recently proposed alkaline treatment (Elert *et al.*, 2015) can overcome this problem, inducing the dissolution of clay minerals and the neoformation of non-expandable mineral phases with cementing properties such as zeolites. These mineralogical changes can lead to improved mechanical and water resistance (*i.e.* increasing the capacity of the structure to withstand the deleterious effects of water of different sources such as rain, condensation, or rising damp) and prolong the lifetime of important monuments and archeological sites (Elert *et al.*, 2015).

Despite the numerous studies focused on the alteration of smectites in highly alkaline environments, some significant gaps in knowledge exist. In general, dioctahedral smectites (*i.e.* montmorillonite and beidellite) have been the focus of experiments investigating clay–cement interactions under nuclear waste-repository conditions at high pH (Gaucher and Blanc, 2006). Only a few studies, in contrast, have been dedicated to

* E-mail address of corresponding author:
kelert@ugr.es
DOI: 10.1346/CCMN.2015.0630601

saponite alteration in highly alkaline environments, even though the potential of this clay as a sealing material in repositories has been recognized for decades (Cuevas *et al.*, 1993). Becerro *et al.* (2009) and Fernandez *et al.* (2014) compared the hydrothermal stability of di- and trioctahedral smectites (including montmorillonite and sepiolite) in contact with hyperalkaline solutions similar in composition to early-stage concrete leachate at pH ≈ 13 and $T \geqslant 175$ºC. As a result of the high experimental *T*, however, pH- and *T*-induced effects on clay-mineral alteration cannot be distinguished and mineralogical changes might occur which are not observed in practical applications. Under repository conditions, for example, the maximum expected *T* at the canister–bentonite interface is limited to ~100ºC (Villar *et al.*, 2006). Another important aspect concerns the experiment duration, which in the cited studies was limited to a maximum of 15 months. Clay dissolution and neoformation of mineral phases at high pH is a relatively slow process, especially at room *T*, and many mineralogical changes can only be observed after prolonged treatment exposure. Most studies, however, are typically limited to less than a year and acceleration of mineral transformation is generally achieved by increasing the experimental *T* (Gaucher and Blanc, 2006). It is, thus, unknown how smectites, both di- and trioctahedral, behave after long-term (>1 y) exposure to highly alkaline solutions at relatively low *T*.

In order to fill some of the aforementioned knowledge gaps, a comparative study on the long-term mineralogical evolution of smectites in highly alkaline solutions was carried out. Particular attention was paid to evaluating the influence of compositional differences on smectite dissolution and formation of new phases. Di- and trioctahedral smectites (*i.e.* montmorillonite and saponite) were, thus, included in this study. Long-term (*i.e.* up to 6 y) batch-reactor experiments were performed at room *T* to ensure that mineralogical changes were only induced by high pH. The effect of solution chemistry was evaluated, comparing mineral dissolution and formation of new phases using 5 M NaOH or 5 M KOH.

The experimental results reported here are part of a laboratory study in which the ultimate goal was to evaluate the possible use of alkaline treatments for the consolidation of earthen architecture (*e.g.* adobe or rammed-earth) made of clay-rich soils (Elert *et al.*, 2015). The outcome of the study, however, may not only have important implications for the alkaline-consolidation treatment proposed here, but also for other technical applications, such as the aforementioned underground storage of nuclear waste.

MATERIALS AND METHODS

Materials and sample preparation

The starting materials included a dioctahedral smectite from Cabo de Gata (Serrata de Nijar, Almería, Spain) and a trioctahedral smectite from the Yunclillos deposit (Toledo, Spain). The two deposits have been characterized extensively, including the thorough analysis (chemical and mineralogical) of their smectitic clays (Huertas *et al.*, 2001; Suarez Barrios *et al.*, 1996). The clay fraction (<2 μm) was separated by centrifugation (KS-8000, Kubota, Tokyo, Japan) and carbonates were eliminated using acetic acid (0.2 N). 5 g of each of the <2 μm fractions of the clays were treated with 100 mL of 5 M NaOH or 5 M KOH solution (all chemicals were reagent grade, Sigma-Aldrich Chemie GmbH, Taufkirchen, Germany). Note that alkaline fluids released by Portland cement have an ionic strength of 0.3–0.7 M (Fernandez *et al.*, 2014). In the experiments reported here, more concentrated solutions were used in order to obtain results in a reasonable period of time and to avoid a reduction in pH over the course of the treatment caused by smectite dissolution (Gaucher and Blanc, 2006). The solutions' pH was ~13. The clay samples were kept in tightly capped polypropylene bottles and stored in the laboratory at 20ºC. Bottles were stirred periodically and samples for analysis were taken at predetermined time intervals (3.5, 6 months, 1, 4, 5, 6 y). Dispersed clay samples (3 mL) collected at each time interval were washed with deionized water until a neutral pH was reached prior to further analysis.

Analytical methods

Elemental analysis of the untreated clay samples was performed using a wavelength dispersive X-ray fluorescence (XRF) spectrometer (S4 Pioneer, Bruker AXS GmbH, Karlsruhe, Germany).

Mineralogical evolution upon alkaline treatment was studied with X-ray diffraction (XRD) using an X′Pert PRO diffractometer (PANalytical B.V., Almelo, The Netherlands). Analyses were performed on oriented mounts which were prepared by pipetting the unreacted and reacted dispersed clay samples on glass slides. Oriented mounts were air-dried at room *T*. Equipment specifications: CuKα radiation, Ni filter, 45 kV voltage, 40 mA current, ¼º divergence slit, ½º anti-scatter slit, 3 to 60º2θ scan range, and 0.05º2θ s^{-1} goniometer speed.

Morphology and qualitative composition of mineral phases were studied using field emission scanning electron microscopy (FESEM, AURIGA, Carl Zeiss SMT, Oberkochen, Germany) coupled with an energy dispersive X-ray spectrometer (EDS, INCA-200, Oxford, Oxforsdshire, UK). Samples were mounted on aluminum stubs using carbon sticky tape and carbon coated prior to analysis. Equipment specifications: Schottky-type field emission gun, 10^{-4} Pa vacuum, 10 kV beam accelerating voltage, and secondary electron imaging mode.

Texture and quantitative composition of untreated and treated samples were examined using transmission electron microscopy (TEM). Two microscopes were used, a Philips CM20 (Amsterdam, The Netherlands)

https://doi.org/10.1346/CCMN.2015.0630601 Published online by Cambridge University Press

Table 1. XRF elemental analysis (wt.%) of the <2 μm fraction of montmorillonite (Mnt) and saponite (Sap).

	SiO_2	Al_2O_3	Fe_2O_3	MgO	TiO_2	Na_2O	K_2O	CaO	LOI	Total
Mnt	58.43	18.04	4.92	4.72	0.19	1.94	1.13	2.20	7.43	99.00
Sap	47.22	4.18	1.60	22.34	0.24	1.94	0.51	0.78	20.62	99.42

equipped with an EDAX solid-state energy dispersive X-ray (EDS) detector and a FEI Titan (Hillsboro, Oregon, USA) with a high-angle annular dark field (HAADF) detector. Samples were dispersed in ethanol, sonicated for 30 s, and deposited on Formvar© carbon-film coated gold grids instead of standard copper grids in order to avoid overlapping of the *K* band of Na and the *L* band of Cu (Drief *et al.*, 2001). Equipment specifications (CM20): lanthanum hexaboride emission source, low-background double-tilt sample holder, 1.33×10^{-6} Pa vacuum, 200 kV accelerating voltage, and bright-field imaging mode. Equipment specifications (Titan): extreme field emission gun (XFEG), analytical double tilt sample holder, 10^{-5} Pa vacuum, 300 kV accelerating voltage, bright-field imaging mode, and 1−15 nm spot size.

Analytical electron microscopy (AEM) analyses were performed on the clay fraction of the treated samples. The AEM was done in scanning TEM mode using a 10 nm diameter beam and 20 nm × 100 nm scanning area. A short counting time of 15 s was used for volatile elements (K and Na) and a longer counting time of 50 s for non-volatile elements. Pure mineral standards were used to obtain *k*-factors allowing X-ray intensities to be corrected by the thin-film method (Lorimer and Cliff, 1976).

Nitrogen sorption isotherms of powdered clay samples before and after alkaline treatment were obtained at 77 K on a Micromeritics TriStar 3000 instrument (Norcross, Georgia, USA). About 0.2 g of sample was degassed at 150ºC for 3 h prior to analysis using a sample degas system (VacPrep 061, Micromeritics, Norcross, Georgia, USA). The surface areas of untreated and treated clay samples were determined using the BET method (Brunauer *et al.*, 1938).

RESULTS

Mineralogical characterization of untreated smectites

Based on XRF data (Table 1) of the <2 μm fraction, the di- and trioctahedral smectites were classified as montmorillonite (Mnt; Whitney and Evans, 2010) and saponite (Sap), respectively. The XRF data were in good agreement with published compositional data for clays from the same deposits (Huertas *et al.*, 2001; Suarez Barrios *et al.*, 1996). The XRD analysis of oriented mounts of the <2 μm fraction revealed a shift of the 001 Bragg peak from ~13 Å (montmorillonite) and ~13.5 Å (saponite) to ~17 Å upon ethylene glycol (EG) solvation and to ~10 Å after heat-treatment at 550ºC (Figure 1). In the saponitic clay, the XRD data further revealed trace amounts of illite (Ilt), and a minor amount of sepiolite (Sep) was detected using TEM. The structural formulae of montmorillonite, saponite, and sepiolite based on TEM-AEM analysis were: $K_{0.03}Na_{0.29}Ca_{0.08}[Al_{1.39}Mg_{0.57}Fe_{0.15}][Si_{3.87}Al_{0.14}]O_{10}(OH)_2$, $K_{0.01}Ca_{0.01}[Al_{0.33}Mg_{2.42}Fe_{0.05}][Si_{3.96}Al_{0.06}]O_{10}(OH)_2$, and $Mg_{3.76}Fe_{0.2}Si_{5.93}O_{15}{\cdot}6H_2O$, respectively.

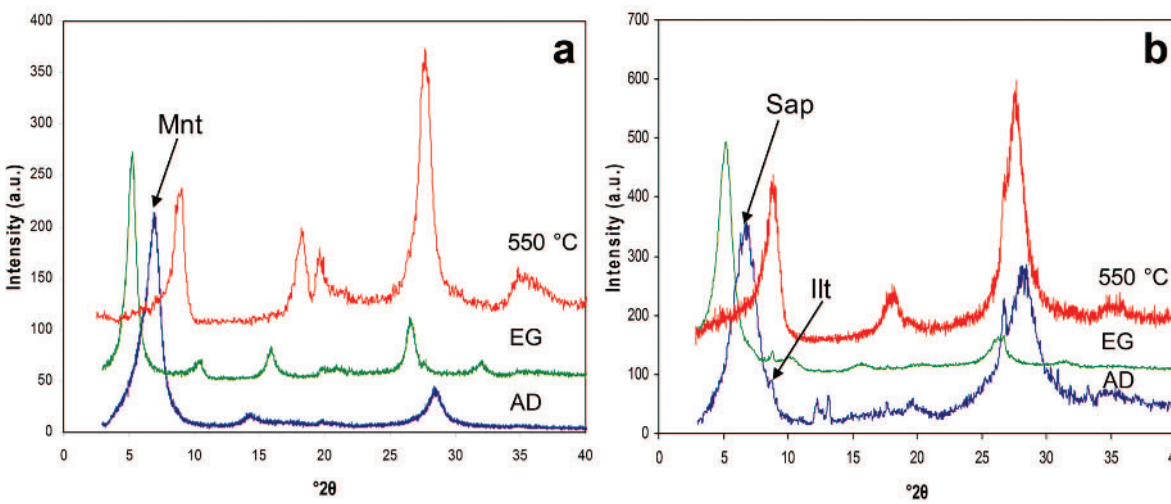

Figure 1. XRD patterns of untreated (a) montmorillonite (Mnt) and (b) saponite (Sap); air-dried (AD), EG-solvated (EG), and heat-treated at 550ºC.

https://doi.org/10.1346/CCMN.2015.0630601 Published online by Cambridge University Press

Mineralogical evolution of montmorillonite treated with 5 M NaOH

The alkaline treatment induced the dissolution of montmorillonite and the neoformation of zeolitic phases at room *T*. In the case of montmorillonite treated with 5 M NaOH solution for 3.5 months, a partial destruction of the clay mineral was indicated by a reduction of the 001 Bragg peak intensity and an increase in peak broadening (Figure 2a). After 6 months, hydroxysodalite (Joint Committee on Powder Diffraction Standards (JCPDS) card no. 410009, $Na_8[AlSiO_4]_6(OH)_2{\cdot}nH_2O$ ($3 \leqslant n \leqslant 4$)) was identified. Furthermore, an additional peak at 14.4 Å was observed which matches the 111 Bragg peak of a faujasite-type zeolite (JCPDS card no. 380232, $(Ca,Na)Al_2Si_{2.5}O_9{\cdot}6.4H_2O$). After 4 y the faujasite-type zeolite was clearly identified and the intensity of the hydroxysodalite Bragg peaks increased also. At this point, the intensity of the 001 montmorillonite Bragg peak decreased further. Differences between diffractograms of EG-solvated and air-dried oriented mounts were minimal, confirming a significant reduction of the clay's swelling capacity as a result of its dissolution and the neoformation of zeolites (Figure 2b). Further alkaline treatment (*i.e.* up to 6 y) resulted in no significant changes.

The FESEM images show the textural features of the montmorillonite sample before (Figure 3a) and after alkaline treatment with 5 M NaOH (Figure 3b–d). Hydroxysodalite crystals had already formed after 3.5 months (Figure 3b). The scarcity and small size of these crystals, however, prevented the acquisition of reliable compositional information using EDS microanalysis. These crystals showed a composition similar to the untreated montmorillonite due to the fact that the electron beam excited signal from surrounding and underlying material (insets, Figure 3a,b). After 4 y of alkaline treatment, hydroxysodalite and faujasite crystals were observed (Figure 3c). Surprisingly, even after 5 years of treatment some of the sample still displayed a morphology which was similar to that of the original montmorillonite (Figure 3d). The chemical composition, however, changed according to EDS microanalysis and the Mg concentration was greater than in the untreated montmorillonite (inset, Figure 3a).

Structural formulae calculated based on TEM-AEM analysis of the <2 μm fraction of montmorillonite treated for 6 y with 5 M NaOH (Table 2) imply that the clay underwent a partial saponitization. This is indicated by a reduction of Si in the tetrahedral sheet and an increase in octahedral Mg, Fe, and octahedral occupancy as compared with the original montmorillonite. Sanchez *et al.* (2006) also reported the formation of a saponitic phase in Febex bentonite, a clay from the same deposit as that used here, treated with 0.5 M NaOH at 200ºC for 540 days. For comparison, the structural formula given by those authors is included (Table 2). Furthermore, mineral phases were detected which had experienced an increase in tetrahedral and octahedral Al, a reduction in Mg and Fe, and an increase in interlayer charge. The chemical changes suggest a transformation of the original montmorillonite into an illite-like phase, but with the dominant interlayer cation being Na as a result of the sodic synthesis environment. Interestingly, even after 6 y of treatment some TEM analyses revealed a composition very similar to that of the original montmorillonite (Table 2, analyses 1–3). This phase experienced only minor substitution of Mg and Fe for octahedral Al, which resulted in a slightly increased interlayer charge.

Mineralogical evolution of montmorillonite treated with 5 M KOH

As in the case of NaOH-treated montmorillonite, clay-mineral dissolution and neoformation of different types of zeolites were observed upon KOH treatment at

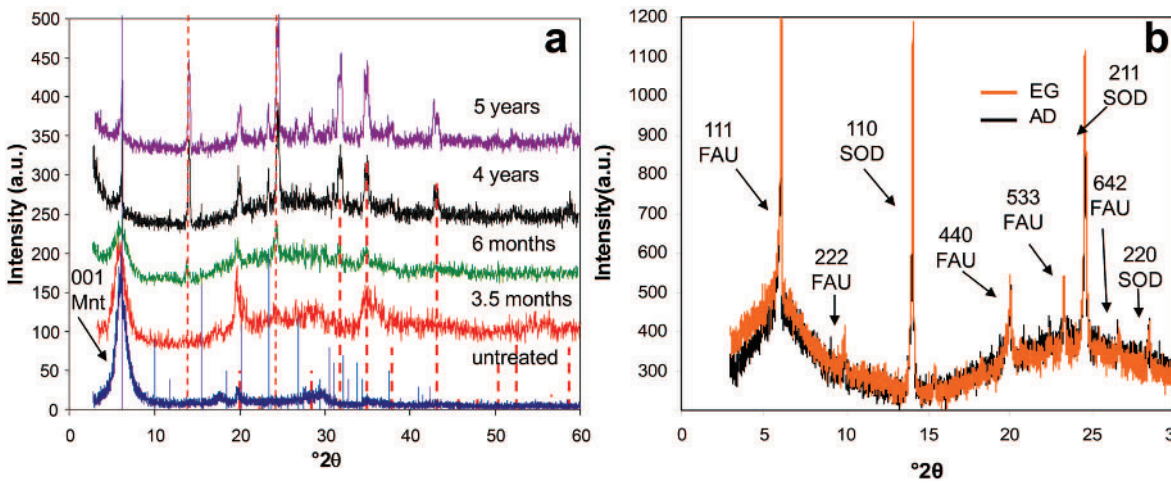

Figure 2. XRD patterns of montmorillonite (Mnt) upon NaOH treatment: (a) mineralogical evolution *vs.* time, solid-line pattern = faujasite (FAU) and dashed-line pattern = hydroxysodalite (SOD); (b) air-dried (AD) and EG-solvated (EG) samples after a 4 y treatment with NaOH.

https://doi.org/10.1346/CCMN.2015.0630601 Published online by Cambridge University Press

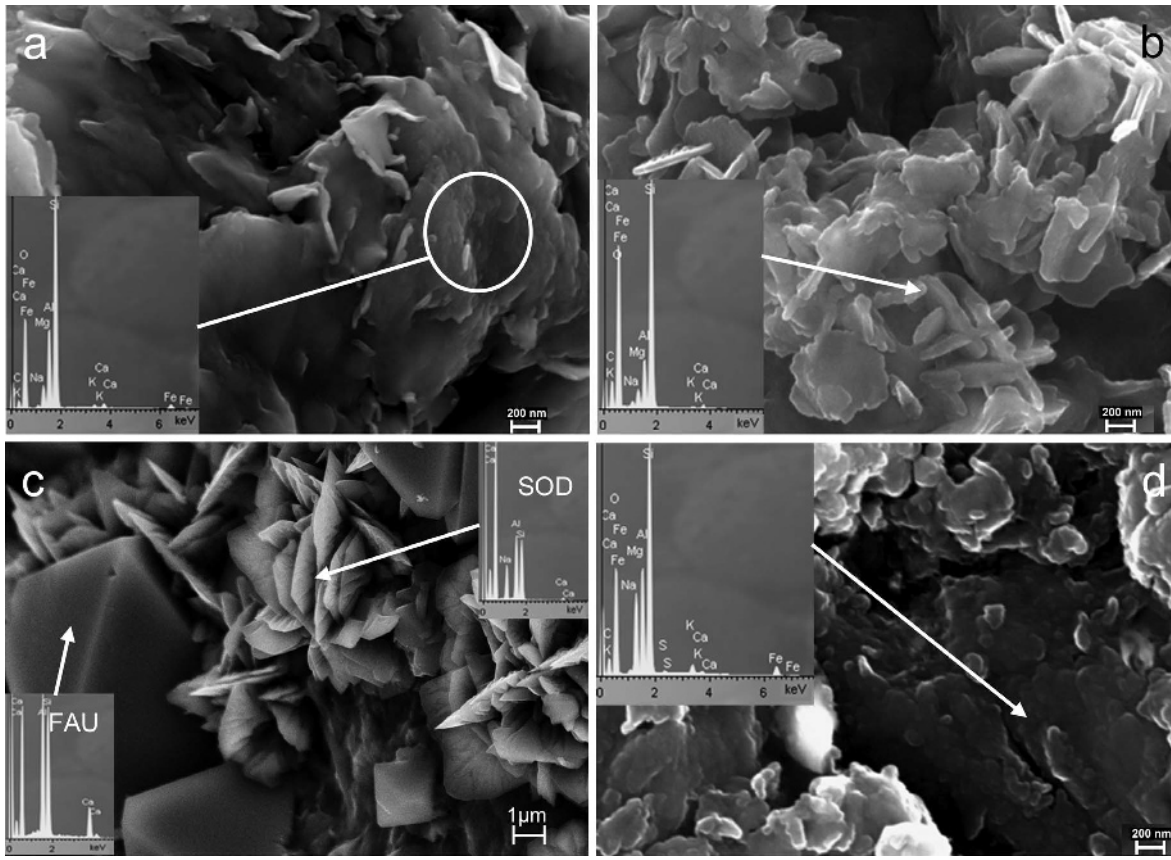

Figure 3. FESEM images of montmorillonite treated with 5 M NaOH: (a) untreated montmorillonite; (b) formation of hydroxysodalite after 3.5 months of treatment; (c) hydroxysodalite (SOD) and faujasite (FAU) after 4 y; and (d) clay sample after 5 y of treatment. EDS spectra inset.

room *T*. A partial destruction of montmorillonite was detected after 3.5 months (Figure 4a). Clear evidence for zeolite formation, however, was first observed after 4 y, when an edingtonite-type zeolite (zeolite K-F, JCPDS card no. 380216, $KAlSiO_4 \cdot 1.5H_2O$) and zeolite K-I (JCPDS card no. 180988, $K_2Al_2SiO_8 \cdot 3.8H_2O$) could be identified. Zeolite formation was accompanied by an intensity reduction of the 001 montmorillonite Bragg peak. Differences between XRD patterns of EG-solvated and air-dried oriented mounts were minimal, confirming

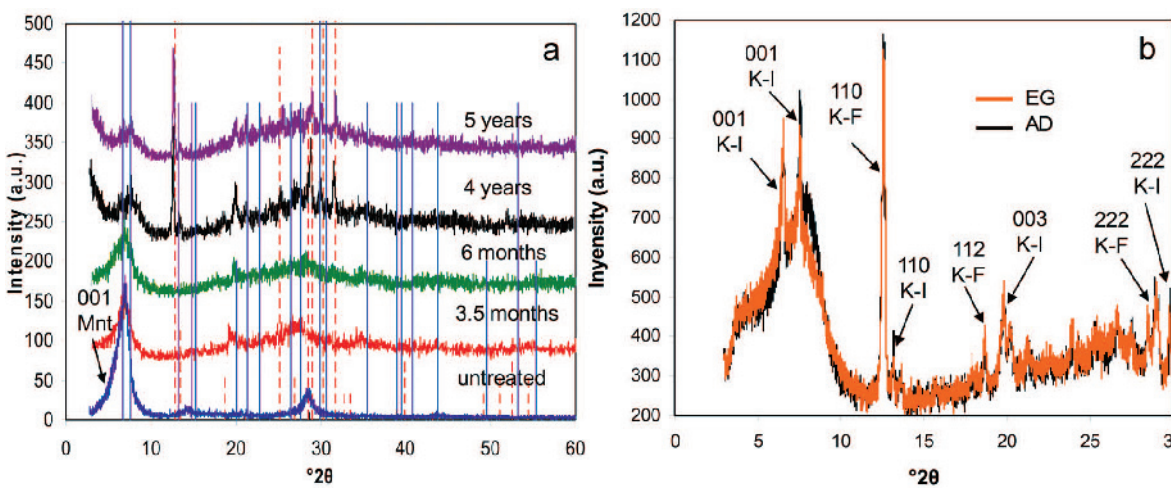

Figure 4. XRD patterns of montmorillonite (Mnt) upon KOH treatment: (a) mineralogical evolution *vs.* time, solid-line pattern = zeolite K-I and dashed-line pattern = zeolite K-F; (b) air-dried and EG-solvated samples after 4 y of treatment with KOH.

https://doi.org/10.1346/CCMN.2015.0630601 Published online by Cambridge University Press

Table 2. TEM-AEM analyses of mineral phases of the <2 μm fraction of montmorillonite treated with 5 M NaOH for 6 y.

	Structural formulae of montmorillonite based on $O_{10}(OH)_2$									
	Si	^{IV}Al	^{VI}Al	Mg	Fe	Σoct.cat.[1]	K	Ca	Na	Σint.cha.[2]
Untreated average[3]	3.87 ±0.10	0.14 ±0.10	1.39 ±0.08	0.57 ±0.03	0.15 ±0.05	2.09 ±0.07	0.03 ±0.02	0.08 ±0.05	0.29 ±0.11	0.48 ±0.19
Dioctahedral smectite										
1	3.88	0.12	1.00	0.64	0.46	2.10	0.09	0.21	0.21	0.72
2	3.90	0.10	1.12	0.67	0.32	2.11	0.01	0.21	0.18	0.61
3	3.98	0.02	1.19	0.62	0.21	2.02	0.07	0.12	0.37	0.68
6 y average	3.92 ±0.05	0.08 ±0.05	1.10 ±0.10	0.64 ±0.03	0.33 ±0.13	2.08 ±0.05	0.06 ±0.04	0.18 ±0.05	0.25 ±0.10	0.67 ±0.06
Saponitization										
4	3.71	0.29	0.97	0.94	0.32	2.23	0.00	0.25	0.27	0.77
5	3.66	0.34	0.82	1.04	0.39	2.25	0.04	0.00	0.19	0.23
6	3.65	0.35	0.86	1.07	0.32	2.25	0.12	0.36	0.00	0.84
7	3.62	0.38	0.98	1.25	0.16	2.39	0.00	0.18	0.20	0.56
8	3.62	0.38	1.00	1.15	0.25	2.40	0.11	0.09	0.20	0.49
9	3.60	0.40	0.85	1.03	0.41	2.29	0.05	0.27	0.16	0.75
10	3.60	0.40	0.93	1.02	0.40	2.35	0.02	0.21	0.16	0.60
11	3.57	0.43	0.80	1.46	0.23	2.49	0.04	0.14	0.23	0.55
12	3.45	0.55	0.90	1.04	0.52	2.46	0.11	0.18	0.00	0.47
13	3.44	0.56	0.79	1.06	0.43	2.28	0.09	0.33	0.22	0.97
14	3.44	0.56	1.06	0.98	0.34	2.38	0.14	0.13	0.17	0.57
15	3.40	0.60	0.82	1.21	0.45	2.48	0.00	0.20	0.18	0.58
16	3.28	0.72	0.69	1.46	0.43	2.58	0.00	0.41	0.00	0.82
6 y Average	3.54 ±0.13	0.46 ±0.13	0.88 ±0.10	1.13 ±0.17	0.36 ±0.16	2.37 ±0.11	0.06 ±0.05	0.21 ±0.11	0.15 ±0.09	0.63 ±0.19
Saponitic phase[4]	3.63	0.37	0.71	1.14	0.10	2.27	0.14		0.55**	0.69
Na-illitization										
18	3.38	0.62	1.67	0.26	0.09	2.02	0.02	0.14	0.59	0.89
19	3.34	0.66	1.58	0.20	0.13	1.91	0.14	0.13	0.17	0.57
20	3.33	0.67	1.91	0.11	0.05	2.07	0.05	0.16	0.23	0.60
21	3.24	0.76	1.44	0.53	0.23	2.20	0.04	0.30	0.18	0.82
22	3.09	0.91	1.99	0.12	0.05	2.16	0.00	0.09	0.40	0.58
23	3.03	0.97	1.67	0.34	0.14	2.15	0.00	0.32	0.31	0.95
6 y average	3.24 ±0.14	0.77 ±0.14	1.71 ±0.21	0.26 ±0.16	0.11 ±0.08	2.09 ±0.11	0.04 ±0.05	0.19 ±0.10	0.31 ±0.16	0.74 ±0.17

[1] Sum of octahedral cations
[2] Sum of interlayer charge
[3] The average structural formula of untreated montmorillonite is included for comparison
[4] The structural formula of a saponitic phase reported by Sanchez *et al.* (2006) is included for comparison
** $M^+ + M^{2+}$

a significant decrease in the clay′s swelling capacity as a result of clay-mineral dissolution and zeolite formation (Figure 4b). Further alkaline treatment caused no further significant changes.

Observations by FESEM confirmed the XRD results. In the montmorillonite sample treated for 4 y with 5 M KOH, a cruciform-shaped/prismatic zeolitic phase and small hexagonal crystals were observed (Figure 5a). These morphologies are in agreement with those of zeolite K-F and zeolite K-I, respectively, which were previously identified using XRD. After 5 y of treatment, EDS microanalysis (Figure 5b inset) revealed a chemical composition consistent with zeolite K-F. As in the case of Na-treated montmorillonite, part of the sample still had a morphology which was comparable with that of the untreated clay (Figure 5c). The FESEM-EDS spectrum (Figure 5c inset), however, revealed changes in the chemical composition, indicating an increase in Mg and K after 5 y of alkaline treatment. The TEM image (Figure 5d) gave additional evidence for the existence of nanosized hexagonal zeolite K-I crystals after 4 y of treatment.

The TEM-AEM analysis of the clay fraction of the montmorillonite sample treated for 6 y with 5 M KOH

https://doi.org/10.1346/CCMN.2015.0630601 Published online by Cambridge University Press

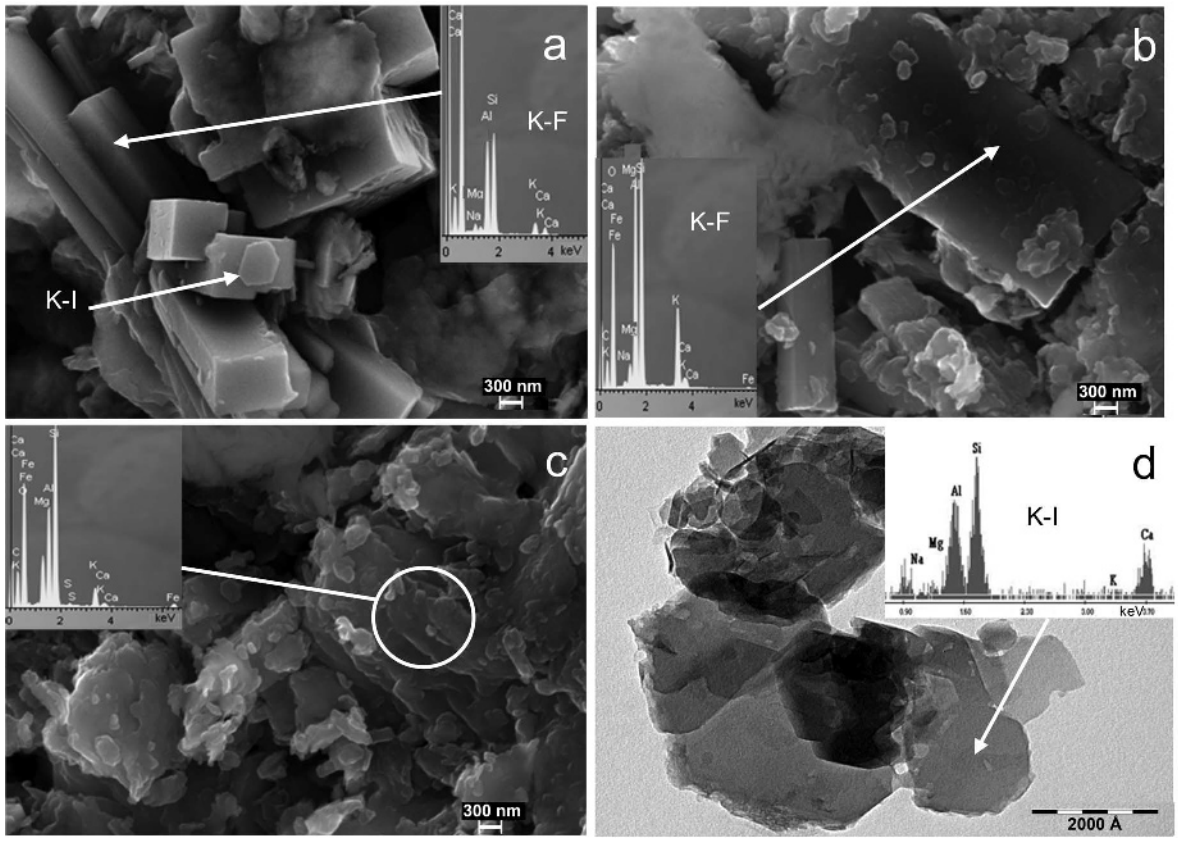

Figure 5. FESEM and TEM images of montmorillonite treated with 5 M KOH: (a) formation of zeolite K-F and K-I after 4 y of treatment; (b) zeolite K-F after 5 y containing mainly K as extraframework cations; (c) clay sample after 5 y of treatment; (d) TEM image of hexagonal zeolite K-I crystals after 4 y. EDS spectra inset.

(Table 3) confirmed FESEM results. The structural formulae indicate different degrees of saponitization which are associated with a gradual decrease in tetrahedral Si and a significant increase in Mg and octahedral occupancy. In some cases, Mg had not only partially replaced octahedral Al but also K, Na, and Ca, and had become the dominant interlayer cation. Only one analysis (Table 4, analysis 1) revealed a chemical composition similar to that of the untreated montmorillonite.

Mineralogical evolution of saponite treated with 5 M NaOH

The XRD analysis showed a decrease in the 001 Bragg peak intensity but no new mineral phases were detected in saponite after 1 y of treatment using 5 M NaOH (Figure 6a). After 5 y of treatment the 001 Bragg peak of saponite shifted from ~13.5 Å to 14.7 Å and additional peaks at 9.7, 7.4, 4.9, 3.7, and 2.9 Å appeared. These changes suggested a transformation of saponite into an interstratified chlorite-saponite. The above-mentioned reflections of the newly formed phase partially fit with corrensite (JCPDS card no.130190, $Mg_8Al_3Si_6O_{20}(OH)_{10}{\cdot}4H_2O$). The 001 reflection of corrensite, however, typically at ~29 Å (Hauff, 1981), was absent, indicating that the sample was not a regularly interstratified 1:1 chlorite-saponite. After EG solvation, the Bragg peak at 14.7 Å shifted to 15.5 Å and not to 17 Å as in the case of the untreated saponite. Heat treatment at 550ºC caused a collapse of this Bragg peak to ~12 Å (Figure 6b). These results are further evidence that saponite has transformed into a randomly interstratified chlorite-saponite. Note that a very similar behavior upon EG solvation and heating was reported for regularly interstratified chlorite-saponite. According to Hauff (1981) and Beaufort and Meunier (1994), the 002 Bragg peak of corrensite expands to ~15.5 Å upon EG salvation and collapses to 12 Å upon heat treatment. Crystalline zeolitic phases were not detected in saponite treated with 5 M NaOH for 6 y.

FESEM images show that even after 6 y of treatment the morphology of large saponite particles did not experience significant modifications compared with the untreated sample (Figure 7a,b). The amount of smaller particles, however, decreased drastically upon alkaline treatment. The EDS microanalysis (Figure 7c inset) showed a composition similar to that of the original clay (Figure 7a inset).

https://doi.org/10.1346/CCMN.2015.0630601 Published online by Cambridge University Press

Table 3. TEM-AEM analyses of the <2 μm fraction of montmorillonite treated with 5 M KOH for 6 y.

Analysis	Structural formulae of montmorillonite based on $O_{10}(OH)_2$									
	Si	^{IV}Al	^{VI}Al	Mg	Fe	Σoct.cat.[1]	K	Ca	Na	Σint.cha.[2]
Untreated average[3]	3.87 ±0.10	0.14 ±0.10	1.39 ±0.08	0.57 ±0.03	0.15 ±0.05	2.09 ±0.07	0.03 ±0.02	0.08 ±0.05	0.29 ±0.11	0.48 ±0.19
Dioctahedral smectite										
1	3.85	0.15	1.59	0.56	0.07	2.22	0.10	0.00	0.00	0.10
Saponitization										
2	3.87	0.13	1.06	1.03	0.16	2.25	0.16	0.05	0.26	0.52
3	3.86	0.14	0.31	2.41	0.11	2.83	0.07	0.04	0.00	0.15
4	3.83	0.17	0.81	1.33	0.28	2.42	0.12	0.12	0.0	0.36
5	3.82	0.18	0.27	2.56	0.11	2.94	0.00	0.00	0.00	0.00
6	3.78	0.22	0.57	1.95	0.07	2.59	0.02	0.23	0.25	0.73
7	3.77	0.23	0.25	2.58	0.13	2.96	0.00	0.00	0.00	0.00
8	3.77	0.23	1.20	0.90	0.19	2.83	0.11	0.11	0.00	0.33
9	3.72	0.28	0.39	2.41	0.13	2.93	0.00	0.00	0.00	0.00
10	3.71	0.29	1.02	1.10	0.27	2.31	0.09	0.14	0.00	0.37
11	3.71	0.29	1.01	1.26	0.16	2.43	0.16	0.11	0.00	0.38
12	3.69	0.31	1.24	0.71	0.30	2.25	0.21	0.11	0.00	0.43
13	3.69	0.31	0.25	2.68	0.09	3.02	0.00	0.00	0.00	0.00
14	3.69	0.31	0.97	1.11	0.26	2.34	0.26	0.14	0.00	0.54
15	3.63	0.37	0.59	1.23	0.24	2.16	0.21	0.16	0.00	0.53
16	3.59	0.41	0.13	2.83	0.15	3.11	0.00	0.00	0.00	0.00
17	3.51	0.49	1.02	1.10	0.22	2.34	0.22	0.09	0.27	0.67
18	3.45	0.55	0.79	1.34	0.34	2.47	0.34	0.15	0.00	0.64
19	3.45	0.55	1.02	1.23	0.27	2.52	0.20	0.09	0.00	0.38
20	3.37	0.63	0.48	1.59	0.17	2.34	0.17	0.32	0.00	0.81
21	3.34	0.66	0.81	1.71	0.32	2.84	0.00	0.00	0.00	0.00
6 y average	3.66 ±0.16	0.34 ±0.16	0.71 ±0.36	1.65 ±0.68	0.20 ±0.08	2.59 ±0.31	0.12 ±0.10	0.09 ±0.09	0.04 ±0.10	0.34 ±0.27

[1] Sum of octahedral cations
[2] Sum of interlayer charge
[3] The average structural formula of untreated montmorillonite is included for comparison.

The TEM-AEM analyses revealed gradual compositional changes in saponite upon alkaline treatment using 5 M NaOH (Table 4). Note that all structural formulae are calculated based on $O_{20}(OH)_{10}$, taking the structural formula of corrensite into account. Changes were detected after just 6 months of treatment: the Si concentration

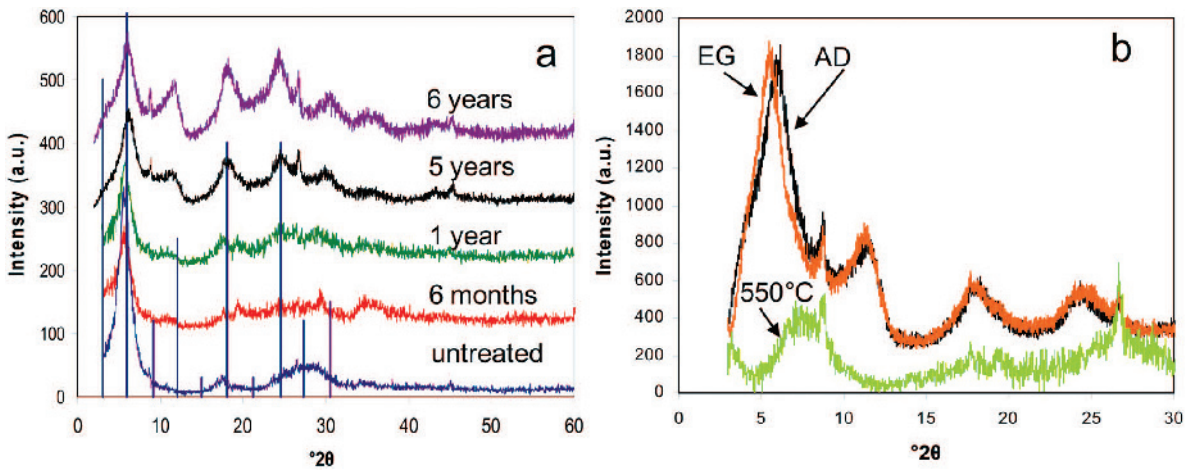

Figure 6. XRD patterns of saponite (Sap) upon NaOH treatment: (a) mineralogical evolution *vs.* time, solid-line pattern = corrensite; (b) air-dried (AD), EG-solvated (EG), and heat-treated (550ºC) samples after 6 y of treatment.

https://doi.org/10.1346/CCMN.2015.0630601 Published online by Cambridge University Press

Table 4. TEM-AEM analyses of saponite treated with 5 M NaOH for 6 months, 1 y, and 6 y.

	Structural formulae of saponite based on $O_{20}(OH)_{10}$									
Analysis	Si	^{IV}Al	^{VI}Al	Mg	Fe	Σoct.cat.[1]	K	Ca	Na	Σint.cha.[2]
Untreated average[3]	9.01 ±0.11	0.00	0.74 ±0.10	5.51 ±0.22	0.11 ±0.03	6.37 ±0.13	0.01 ±0.02	0.01 ±0.01	0.00	0.02
1	8.84	0.00	0.87	5.75	0.08	6.70	0.00	0.16	*	**
2	8.25	0.00	0.81	7.09	0.12	8.02	0.00	0.04	*	**
3	8.13	0.00	0.87	7.43	0.00	8.30	0.00	0.00	*	**
4	8.03	0.00	0.77	7.56	0.12	8.45	0.00	0.09	*	**
6 months average	8.31 ±0.36	0.00	0.83 ±0.05	6.96 ±0.83	0.08 ±0.06	7.87 ±0.80	0.00	0.07 ±0.07	*	**
5	8.09	0.00	0.99	7.02	0.12	8.13	0.08	0.13	*	**
6	7.97	0.03	0.86	7.51	0.08	8.45	0.04	0.09	*	**
7	7.56	0.44	0.59	8.05	0.17	8.81	0.09	0.04	*	**
1 y average	7.87 ±0.28	0.16 ±0.25	0.81 ±0.20	7.53 ±0.52	0.12 ±0.05	8.46 ±0.34	0.07 ±0.03	0.09 ±0.05	*	**
8	7.91	0.09	0.96	8.06	0.25	9.27	0.00	0.00	0.00	**
9	7.66	0.34	0.75	7.79	0.21	8.75	0.00	0.00	0.00	**
10	7.60	0.40	0.75	7.64	0.31	8.70	0.00	0.00	0.00	**
11	7.59	0.41	0.70	7.80	0.24	8.74	0.00	0.00	0.00	**
12	7.53	0.47	0.61	8.04	0.20	8.85	0.00	0.00	0.00	**
13	7.49	0.51	0.57	8.12	0.22	8.91	0.00	0.00	0.00	**
14	7.47	0.53	0.81	7.73	0.25	8.79	0.00	0.00	0.00	**
15	7.38	0.62	0.76	7.84	0.25	8.85	0.00	0.00	*	**
16	7.37	0.63	0.67	7.70	0.43	8.80	0.00	0.00	0.00	**
17	7.18	0.82	0.36	8.66	0.17	9.19	0.00	0.00	*	**
6 y average	7.52 ±0.20	0.48 ±0.20	0.69 ±0.16	7.94 ±0.30	0.25 ±0.07	8.89 ±0.19	0.00	0.00	**	**

[1] Sum of octahedral cations
[2] Sum of interlayer charge
[3] The average structural formula of untreated saponite based on $O_{20}(OH)_{10}$ is included for comparison
* not analyzed
** not calculated

decreased while Al, Fe, and especially Mg increased. These results confirm that saponite experienced a chloritization process and transformed into a randomly interstratified chlorite-saponite. Compared with published data for regular 1:1 chlorite-saponite interstratification (Brigatti and Poppi, 1984; Newman and Brown, 1987), the Si concentration is still quite high and the Al concentration too small after 6 y of treatment. This indicates that the chloritization process was not complete and that the newly formed phase had a saponite/chlorite layer ratio which was >1:1. The high-resolution TEM image (Figure 7d) provides evidence for the presence of chlorite layers with 14 Å *d* spacing sandwiched between saponite layers. Note that saponite layers contracted to 10 Å upon exposure to the electron beam.

Mineralogical evolution of saponite treated with 5 M KOH

The XRD data revealed a shift of the 001 Bragg peak of saponite from ~13.5 Å to ~14.5 Å. The formation of a new mineral phase, however, was not detected, even after 6 y of treatment at room *T* (Figure 8a). Illite was still

Figure 7 (*facing page*). FESEM (a) and TEM (b) image of untreated saponite (Sap) and sepiolite (Sep), respectively; (c) FESEM image after 6 y of treatment with 5 M NaOH; (d) HRTEM image of randomly interstratified chlorite-saponite after 6 y of treatment with 5 M NaOH. Note that (001) saponite layers collapse to 10 Å *d* spacing upon electron beam irradiation, whereas (001) chlorite layers (*d* spacing = 14 Å) are not affected by the electron beam; (e) FESEM image of an amorphous phase present after 6 y of treatment with 5 M KOH; (f) FESEM image of saponite after 6 y of treatment with 5 M KOH. EDS spectra inset; (g) TEM image of an amorphous phase present after 6 y of treatment with 5 M KOH (SAED pattern in inset); (h) Annular dark-field STEM microanalysis showing elemental distribution corresponding to the TEM image in part g.

https://doi.org/10.1346/CCMN.2015.0630601 Published online by Cambridge University Press

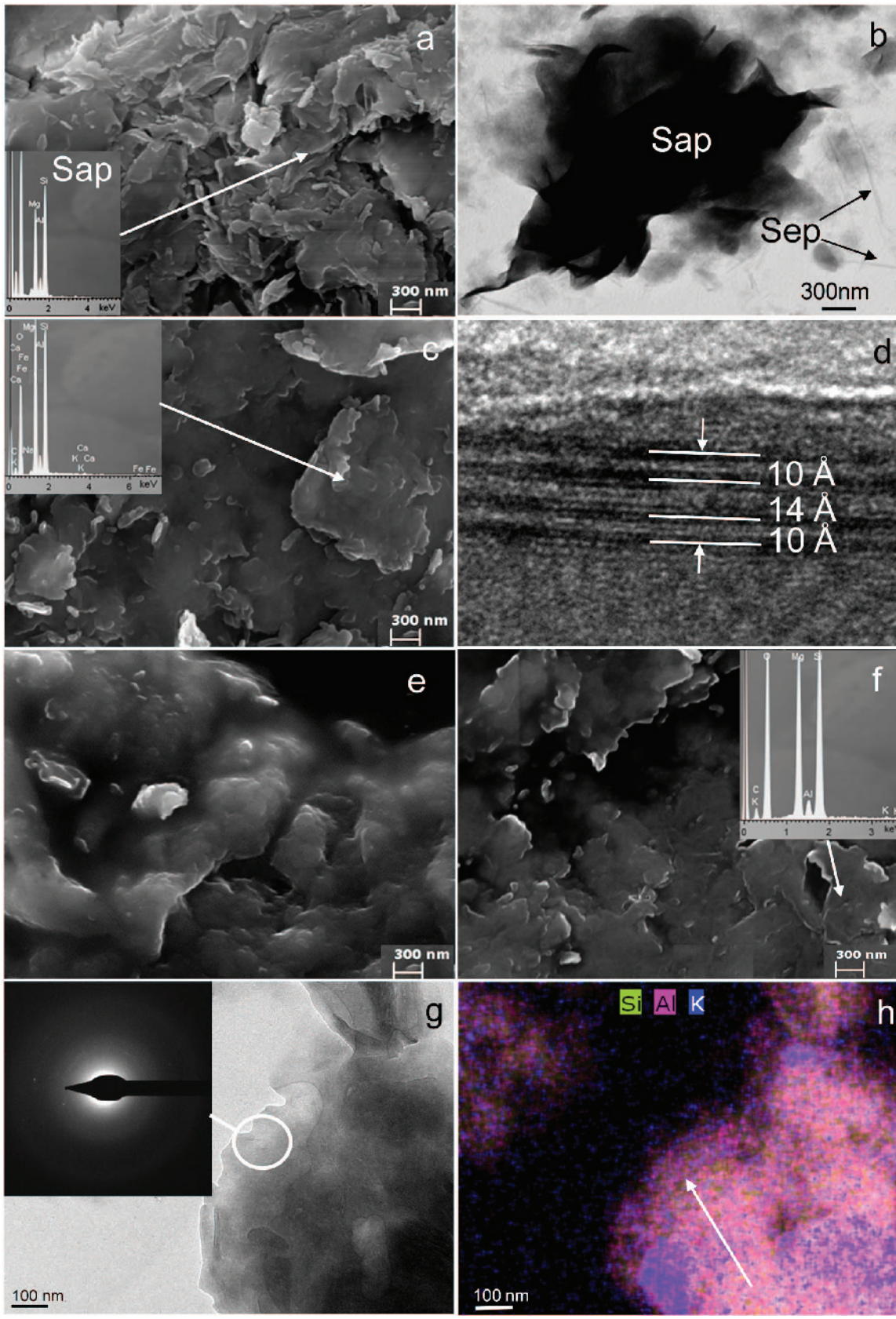

https://doi.org/10.1346/CCMN.2015.0630601 Published online by Cambridge University Press

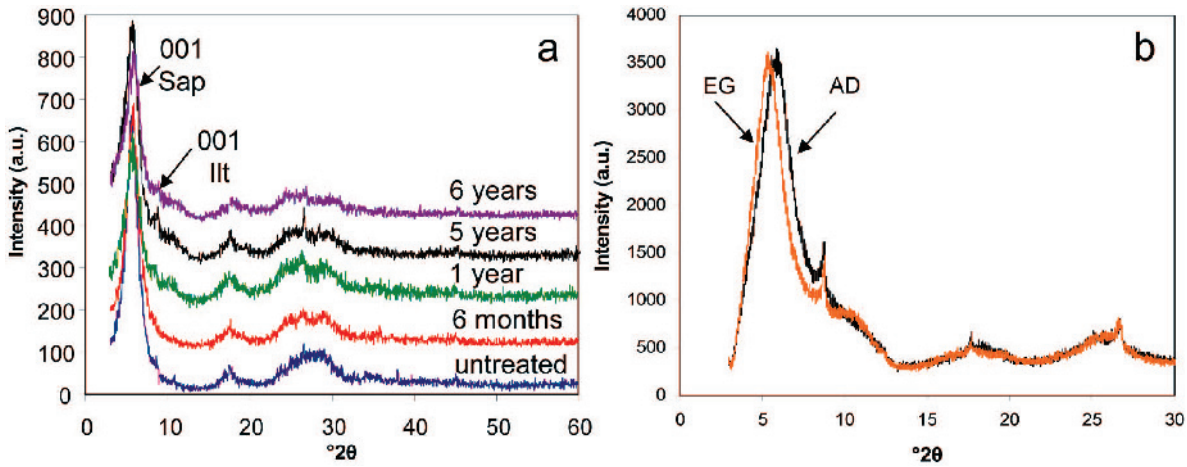

Figure 8. XRD patterns of saponite (Sap) upon KOH treatment: (a) mineralogical evolution *vs.* time, Ilt = illite; (d) air-dried and EG-solvated samples after 6 y.

detected and its 001 Bragg peak intensity actually seemed to have increased slightly. Cuevas Rodriguez (1993), who studied the hydrothermal stability of saponites from the same area, interpreted this phenomenon as a recrystallization process experienced by illite in the presence of K, leading to an increased degree of crystallinity. After EG solvation of the sample treated for 6 y, the 001 saponite Bragg peak still shifted from ~14.5 Å to ~16.7 Å (Figure 8b), suggesting that the clay had not experienced significant changes in swelling capacity.

Using FESEM analysis, a partial dissolution of the sample affecting smaller clay particles and the neoformation of an amorphous phase which covered the surrounding saponite particles (see TEM-SAED results, below) were observed after 6 y of treatment (Figure 7e). Note that even after 6 y of treatment with 5 M KOH, some of the sample showed a chemical composition which was similar to the untreated saponite (Figure 7f inset). No crystalline zeolitic phase was observed in the KOH-treated saponite.

Analysis by TEM confirmed the amorphous character of this newly formed phase (Figure 7g inset). This phase was composed primarily of Si, leading to an increase in Si concentration at the outer rim (Figure 7h, arrow). Note that some zones of the map contained high concentrations of Al and K, probably due to the presence of illite impurities.

The TEM-AEM analysis confirmed XRD and FESEM results, illustrating only minor compositional changes in saponite upon treatment with 5 M KOH (Table 5). Note that the Si concentration of the untreated saponite is slightly higher and the Mg concentration slightly lower than those reported for saponite (Newman and Brown, 1987). This discrepancy is caused by the presence of sepiolite which interferes with the TEM-AEM analysis (Cuevas *et al.*, 2001). Upon KOH treatment, a reduction in Si and a concomitant increase of Mg and octahedral occupancy were observed. The Al concentration, however, remained practically unchanged. After 6 y of treatment, the clay mineral's composition was nearly identical to that of the untreated saponite (Table 5, analysis 1–5), indicating a relatively small effect of the treatment with 5 M KOH on the trioctahedral clay.

Nitrogen-sorption measurements of montmorillonite and saponite

The BET surface area measurements provided additional evidence for the more pronounced textural changes experienced by montmorillonite upon alkaline treatment as compared to saponite. The experimentally unaltered montmorillonite and saponite had BET surface areas of 63.6 m^2/g and 143.8 m^2/g, respectively (Table 6). These values are in agreement with reported data for clays from the same deposits (60 m^2/g (Sanchez *et al.*, 2006) and 161 m^2/g (Prieto *et al.*, 1999), respectively).

Montmorillonite treated with either 5 M NaOH or 5 M KOH experienced a surface area increase of ~100%. In saponite, on the other hand, surface area changes of <10% were observed which are well within the experimental error of this technique (Table 6).

The nitrogen sorption isotherms of both smectites were identified as type II, common for smectites (Rouquerol *et al.*, 1998) with a hysteresis loop of type H3, caused by aggregates of plate-like particles and indicative of the presence of fine, slit-shaped pores (Sing *et al.*, 1985). A significant reduction of the hysteresis loop was observed for alkaline-treated montmorillonite (Figure 9a), whereas the hysteresis loop of saponite did not experience any changes (Figure 9b).

DISCUSSION

Comparison of the mineralogical evolution of montmorillonite and saponite upon alkaline treatment

Experimental results revealed a very different mineralogical evolution of montmorillonite and saponite upon

https://doi.org/10.1346/CCMN.2015.0630601 Published online by Cambridge University Press

Table 5. TEM-AEM analyses of saponite treated with 5 M KOH for 6 months and 6 y.

	Structural formulae of saponite based on $O_{10}(OH)_2$									
	Si	^{IV}Al	^{VI}Al	Mg	Fe	Σoct.cat.[1]	K	Ca	Na	Σint.cha.[2]
Untreated average[3]	3.96 ±0.11	0.06 ±0.08	0.33 ±0.10	2.42 ±0.21	0.05 ±0.03	2.80 ±0.13	0.01 ±0.02	0.01 ±0.01	0.00	**
1	3.91	0.09	0.21	2.66	0.02	2.89	0.02	0.00	0.11	**
2	3.83	0.11	0.17	2.79	0.06	3.02	0.06	0.00	0.06	**
3	3.56	0.31	0.00	3.27	0.07	3.34	0.06	0.02	0.00	**
4	3.64	0.33	0.00	2.98	0.07	3.05	0.06	0.04	0.20	**
5	3.54	0.32	0.00	3.01	0.11	3.12	0.09	0.06	0.37	**
6 months average	3.70 ±0.17	0.23 ±0.12	0.08 ±0.11	2.94 ±0.23	0.07 ±0.03	3.10 ±0.17	**	**	**	**
8	3.96	0.04	0.28	2.50	0.09	2.87	0.00	0.00	0.00	**
9	3.95	0.05	0.32	2.49	0.05	2.86	0.00	0.00	0.00	**
10	3.85	0.15	0.32	2.51	0.07	2.90	0.00	0.00	0.00	**
11	3.84	0.16	0.22	2.66	0.07	2.95	0.00	0.00	0.00	**
12	3.78	0.22	0.27	2.51	0.11	2.89	0.14	0.00	0.00	**
13	3.76	0.24	0.23	2.70	0.05	2.98	0.00	0.00	0.00	**
14	3.73	0.27	0.28	2.63	0.07	2.98	0.00	0.00	0.00	**
15	3.73	0.27	0.11	2.77	0.06	2.94	0.02	0.04	0.16	**
16	3.71	0.29	0.09	2.77	0.06	2.92	0.02	0.06	0.22	**
17	3.70	0.30	0.10	2.76	0.05	2.91	0.07	0.04	0.21	**
18	3.70	0.30	0.22	2.70	0.09	3.01	0.00	0.00	0.00	**
19	3.61	0.38	0.00	3.06	0.09	3.15	0.06	0.00	0.00	**
20	3.58	0.42	0.13	2.91	0.09	3.13	0.00	0.00	0.00	**
21	3.55	0.42	0.00	3.05	0.06	3.11	0.02	0.04	0.22	**
22	3.54	0.46	0.01	3.02	0.14	3.17	0.04	0.00	0.00	**
23	3.46	0.48	0.00	3.25	0.09	3.34	0.02	0.00	0.00	**
6 y average	3.72 ±0.14	0.28 ±0.13	0.16 ±0.12	2.77 ±0.23	0.08 ±0.02	3.01 ±0.14	**	**	**	**

[1] Sum of octahedral cations
[2] Sum of interlayer charge
[3] The average structural formula of untreated saponite is included for comparison
** not calculated.

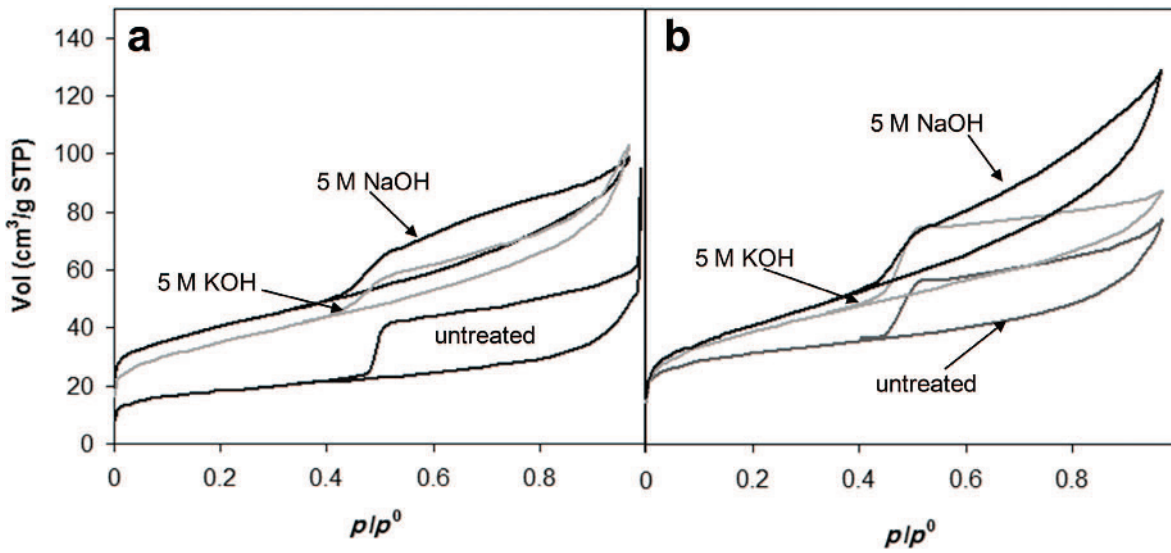

Figure 9. Nitrogen adsorption isotherms (a) untreated montmorillonite and montmorillonite treated for 5 y with 5 M NaOH and 5 M KOH; and (b) untreated saponite and saponite treated for 6 y with 5 M NaOH and 5 M KOH.

https://doi.org/10.1346/CCMN.2015.0630601 Published online by Cambridge University Press

Table 6. BET surface areas of smectites treated with 5 M NaOH and 5 M KOH.

Time	Surface area (m^2/g)			
	– Montmorillonite –		Saponite	
	NaOH	KOH	NaOH	KOH
0	63.58	63.58	143.75	143.75
6 months	82.81	60.24	154.36	153.82
5 y	141.39	123.22	–	–
6 y	–	–	144.77	136.81

alkaline treatment at room *T* which influenced the swelling capacity of the clays to a significant degree. Montmorillonite treated with 5 M NaOH or 5 M KOH dissolved readily. In these samples zeolite formation was detected and only a small amount of expandable clays remained, revealing a significant reduction in swelling capacity. NaOH-treated saponite, in contrast, showed no zeolite formation and transformed gradually into a randomly interstratified chlorite-saponite which experienced significant expansion upon EG solvation. The KOH treatment of saponite resulted in the limited formation of a Si-rich amorphous phase, identified with FESEM/TEM, which did not alter the swelling capacity of the clay.

From these observations the saponite can be inferred to present a lower degree of 'alterability' than montmorillonite in alkaline environments. Further proof for the greater persistence of saponite under the experimental conditions is given by the fact that a saponitic phase was identified as one of the transformation products in the case of NaOH-treated montmorillonite. This finding is in agreement with results reported by Ramirez *et al.* (2002) and Sanchez *et al.* (2006). Under natural conditions, saponitization of dioctahedral smectite at high pH has also been observed (Pozo Rodriguez and Casas Sainz de Aja, 1992). Additionally, Bristow *et al.* (2009) commented on the importance of a high pH (~9 or higher) for the formation of trioctahedral smectites at appreciable rates.

Surface-area measurements confirmed that montmorillonite underwent significant textural changes, resulting in an important increase in surface area which was related to the formation of faujasite with a reported surface area of 400 m^2/g (Sutarno and Arryanto, 2007). The hydroxysodalite also detected will not contribute to a surface-area increase, having a reported surface area of only 22.8 m^2/g (Li *et al.*, 2007). The relation between zeolite formation and surface-area increase is not as evident in the case of montmorillonite treated with KOH. The pores of zeolite K-I and K-F (pore size: 0.26 nm; Breck, 1974) should not be accessible to nitrogen, which only has access to pores with a size of $\geqslant$~0.5 nm (Groen *et al.*, 2003). Accordingly, the reported BET surface area of zeolite K-F is only 20.2 m^2/g (Miyaji *et al.*, 2009). The presence of Ca, however, in addition to K in the experimentally produced zeolites K-I and K-F may have resulted in a larger surface area. According to Csicsery (1984), monovalent cations can block pores and restrict the pore size to <~0.4 nm, while divalent cations only occupy every second cationic position, leaving space for larger molecules to enter, including N_2. This would explain why montmorillonite experienced a surface-area increase of nearly 100% after 5 y of treatment with 5 M KOH.

In the case of saponite, important surface-area changes were not observed. Note that chloritization of saponite would actually be expected to cause a surface-area decrease, the reported surface area for a regularly interstratified 1:1 chlorite-saponite (corrensite) being 36 m^2/g (Siegel *et al.*, 1990). Thus, only limited chloritization can be inferred as having occurred in NaOH-treated saponite.

Modifications of the shape of the hysteresis loop of the nitrogen isotherm can give important information on textural changes experienced by clays upon alkaline treatment. The hysteresis loop reduction detected in treated montmorillonite is a result of a partial dissolution of the plate-like clay particles and the neoformation of zeolites of equant shape, both resulting in a decrease of fine, slit-shaped pores. The hysteresis loop of saponite, in contrast, remained basically unchanged during these experiments, indicating that the transformation experienced by this clay did not result in major textural modifications. These observations were in agreement with FESEM analysis results showing the persistence of plate-like aggregates of saponite particles after prolonged alkaline treatment which give rise to the aforementioned slit-shaped pores.

The contrasting textural and mineralogical evolution of montmorillonite and saponite exposed to highly alkaline solutions can be explained considering differences in chemical composition and charge distribution between them. The greater resistance of trioctahedral smectites, namely saponite, hectorite, and Laponite®, compared with that of dioctahedral smectites such as montmorillonite and beidellite when treated with alkaline solutions at 300ºC was reported by Becerro *et al.* (2009). Those authors suggested that the full occupancy of the octahedral sheet by mainly Mg^{2+} (*i.e.* forming a brucite sheet) would be decisive for the greater resistance of the former group of clays under alkaline attack. Pokrovsky and Schott (2004) demonstrated that dissolution rates of brucite were drastically reduced as

https://doi.org/10.1346/CCMN.2015.0630601 Published online by Cambridge University Press

pH increased from 8 to 12. Using acid/base titration, the same authors determined the point of zero charge (PZC) of brucite to be pH ~11. According to the same authors the concentration of deprotonated >MgOH groups was only significant at pH >12. In the case of montmorillonite, Al is the dominant octahedral cation, forming a gibbsite sheet. The gibbsite dissolution rate increases significantly at pH >10 (Nagy, 1995). The PZC of gibbsite is pH ~9 (Karamalidis and Dzombak, 2010) and complete deprotonation is achieved at pH ~12 (Rozalen *et al.*, 2009). Note that the PZC marks the pH at which the solubility of a particular phase is at its minimum (Somasundaran and Agar, 1967). Considering that dissolution rates are proportional to the concentration of negatively charged surface sites (*i.e.* deprotonated $>MgO^-$ and $>AlO^-$ sites) at high pH (Brady and Walther, 1989; Stumm, 1997), the dissolution of brucite sheets can be expected to occur at lower rates than the dissolution of gibbsite sheets under equally high pH conditions.

Differences in charge distribution may also contribute to the observed variations in reactivity of di- and trioctahedral smectites. The surface of the tetrahedral sheet of 2:1 phyllosilicates contains ditrigonal cavities with reactive siloxane functional groups. Depending on the nature of the electronic charge distribution (*i.e* octahedral or tetrahedral substitution), these groups can form complexes with water-solvated or unsolvated interlayer cations (*i.e.* outer- or inner-sphere complexes). Outer-sphere complexes involving electrostatic bonding are less stable than inner-sphere complexes involving covalent bonding or a combination of covalent and electrostatic bonding (Sposito, 1984). As a result of weaker bonds between the tetrahedral sheet and the interlayer cation associated with octahedral substitution, the entry of water molecules into the interlayer space and, thus, the hydration of interlayer cations are facilitated in the case of Na-montmorillonite (Norrish, 1954). Clay layers will be forced apart when the number of hydration layers around the cation increases, offering a greater surface area for reaction (*i.e.* dissolution). In contrast, tetrahedral substitution leads to stronger bonds, limiting interlayer cation hydration. This is exemplified by Na-beidellite which displays predominantly tetrahedral substitution. Because Na cations are strongly bonded to the clay surface and do not hydrate easily beyond the one-layer hydrate, swelling of Na-beidellite is limited (Hensen and Smit, 2002). A similar effect should also occur in saponite, where a restricted access of water molecules into the interlayer space will limit separation of clay layers, thus, hampering the dissolution process under alkaline conditions.

Newly formed phases in montmorillonite upon alkaline treatment

In the case of montmorillonite, mineralogical changes were dominated by the neoformation of various zeolitic phases, accompanied to a minor degree by the transformation into high-charge clay minerals or saponitic phases.

The zeolitic phases detected in treated montmorillonite are in agreement with previously reported data of zeolites synthesized under similar pH conditions using clays as starting materials (Barrer *et al.*, 1968; Bauer *et al.*, 1998; Felsche *et al.*, 1986). Published results indicate that the cation of the mineralizing solution, either Na^+ or K^+, determines the type of zeolite formed upon alkaline treatment of clays. Barrer (1982) discussed the structure-directing role of cations and concluded that sodic environments favored the formation of faujasite and sodalite hydrates, whereas treatments with KOH resulted in the formation of zeolite K-F (edingtonite-type zeolite) and zeolite K-I.

Apart from zeolite formation, Na-illitization and saponitization of the remaining clay fraction was detected in the experimentally altered montmorillonite upon NaOH treatment. Illitization has been identified as a common transformation process of dioctahedral smectites (Eberl *et al.*, 1993; Bauer and Velde, 1999; Drief *et al.*, 2002). Generally, illitization is linked to the presence of K and results in an important increase in tetrahedral charge due to isomorphic substitution (Cuadros, 2008). Here, a similar process in NaOH-treated montmorillonite was observed. The resulting phase, however, contained Na as the dominant interlayer cation as a result of the high concentration of Na in the mineralizing solution. In some cases the structural formulae based on TEM-AEM analysis (Table 2, analyses 18–20) could actually be interpreted as a high-charge beidellite. The formation of beidellite upon alkaline treatment at room *T* (Karnland *et al.*, 2007) and upon hydrothermal alteration of montmorillonite (Meunier *et al.*, 1998) has been observed previously. According to Mosser-Ruck and Cathelineau (2004), beidellitization can be regarded as an initial step of illitization.

Saponitization of dioctahedral smectite is generally associated with an increase in tetrahedral charge as well as in octahedral Mg (Sanchez *et al.*, 2006). The experimental results reported here indicate that saponitization is a slow process and, after 6 y of treatment, the identified product phase still lacked Mg compared to the commonly reported saponite compositions (Newman and Brown, 1987) and was, thus, interpreted as an intermediate phase (*i.e.* di- + tri-octahedral smectite intergrowth) during saponite formation.

Newly formed phases in saponite upon alkaline treatment

The NaOH-treated saponite transformed into a randomly interstratified chlorite-saponite which can be considered as a transitional phase towards corrensite. Corrensite, in turn, is often identified as an intermediate phase in the smectite–chlorite transformation (Beaufort

https://doi.org/10.1346/CCMN.2015.0630601 Published online by Cambridge University Press

et al., 1997; Brigatti and Poppi, 1984; Bristow *et al.*, 2009; Murakami *et al.*, 1999). The results reported here indicate that chloritization can be a relatively slow process. After 6 y of alkaline treatment, the saponite had only transformed into a randomly interstratified chlorite-saponite which still showed an important swelling capacity upon EG solvation.

Compositional changes in the KOH-treated saponite were only minor after 6 y, and the structural formula based on TEM-AEM data was still consistent with that of saponite. The detected newly formed amorphous phase acted as a sink for Si which was released during saponite dissolution. Note that the release of Si from saponite followed by the precipitation of amorphous silica would enable Mg enrichment of the remaining saponitic phase. The XRD analysis revealed a shift of the 001 Bragg peak of saponite from ~ 13.5 to ~14.5 Å upon alkaline treatment, which was probably a result of the formation of some brucite sheets. Unlike in the case of NaOH-treated saponite, clear evidence for chloritization could not be detected in the sample treated with KOH.

Interestingly, no crystalline zeolitic phases were observed in saponite upon alkaline treatment. The reason for the absence of zeolitic phases may be twofold. On the one hand, the comparatively low Al concentration of saponite may inhibit zeolite crystallization. The synthesis of low-aluminum zeolites (*i.e.* high-silica zeolites, Si/Al > 5) generally requires the use of organic cations such as alkylammonium which act as mineralizers and structure-directing agents, or by the addition of zeolite seeds (Davis and Lobo, 1992; Moliner, 2012). Furthermore, the required reaction *T* is greater than in the case of low-silica zeolites (Barrer, 1982; Davis and Lobo, 1992). In addition, the required reaction time becomes longer with increasing Si content of the starting material (Barth-Wirsching and Höller, 1989). Kovalchuk *et al.* (2008) presented data on the activation of fly-ash with NaOH which showed that zeolites did not form at a Si/Al ratio >3.5.

On the other hand, the large Mg concentration in the case of saponite may also hinder zeolite nucleation. Breck (1974) reported on experimental simulation of the action of sea water on basalt weathering. In the presence of Mg, montmorillonite was the main product, whereas an analcime-type zeolite formed in the absence of Mg. Gottardi (1989) came to the same conclusion, proposing that only sheet silicates (*i.e.* clay minerals) were obtained when Mg was added to a mixture intended for zeolite synthesis. The reason for the inhibiting effect of Mg on zeolite nucleation is, however, not clear. According to Kirov and Filizova (2012), Mg cannot act as a template and cannot form zeolites on its own as a result of its large and stable hydration shell. In any case, the effect of Mg on zeolite nucleation does not seem to be the same for all zeolite types. Singh and Dutta (1998) reported on the inhibiting effect of Mg on faujasite nucleation during the initial stage of synthesis whereas zeolite P1 crystallization was not affected by its presence. Furthermore, many natural zeolites such as faujasite, erionite, and offretite contain Mg as extra-framework cations (Gottardi, 1989). Small concentrations of Mg are permissible in zeolite synthesis solutions in any case. This can be inferred from the fact that zeolites crystallized when montmorillonite was used as a starting material which contained Mg, but in a concentration almost six times less than in the unaltered saponite used in the present study. A systematic study would be required in order to elucidate unambiguously the ultimate reason for the absence of zeolites in alkaline-treated saponite.

Implication for earthen-architecture consolidation and nuclear-waste storage

The experimental results here show that montmorillonite lost almost completely its swelling capacity upon alkaline treatment with 5 M NaOH or 5 M KOH solutions. This finding indicates that in the case of earthen structures containing montmorillonite, an alkaline consolidation treatment would certainly result in improved water resistance because dioctahedral smectites transform into zeolites which do not expand when in contact with water (Mumpton, 1985). This is consistent with the results reported for improved water resistance of alkaline-treated adobe blocks made of soil from the Alhambra Formation which contained dioctahedral smectites (Elert *et al.*, 2015). Furthermore, the formation of zeolites is expected to improve mechanical properties of clays and soils. Slaty *et al.* (2013) obtained a cement clinker replacement with a compressive strength of up to 23 MPa based on kaolinite reacted with NaOH at 80ºC for 24 h. The authors related the high compressive strength of this material to the formation of zeolites and feldspathoids including phillipsite, natrolite, and hydroxysodalite which fill pore spaces and bind the matrix. Roy (1999) suggested that the high durability of pozzolanic Roman cement mortars could be related to the presence of zeolites such as analcime.

The swelling capacity of saponite, in contrast, was only reduced to a certain degree upon alkaline treatment (Figures 6b and 8b), calling into question the effectiveness of an alkaline treatment for the consolidation of earthen architecture containing significant amounts of trioctahedral smectites, because the water resistance is not expected to improve significantly. As a sealing material in hazardous-waste repositories, however, saponite can be considered as a viable alternative to the more frequently used dioctahedral smectites. Under repository conditions, the limited and slow transformation of saponite into corrensite-type minerals will be beneficial to preserving the clays' swelling capacity and, thus, its effectiveness as a sealing material. The lower alterability of saponitic clays in hyperalkaline fluids as compared to dioctahedral smectites was pointed out by

https://doi.org/10.1346/CCMN.2015.0630601 Published online by Cambridge University Press

Fernandez *et al.* (2014). The loss of swelling capacity observed here as a result of zeolite formation in montmorillonite, in contrast, limits the effectiveness of the clay as a sealing material in waste repositories as a result of increased permeability. The excellent adsorbent and cation-exchange properties of zeolites, however, can be regarded as a positive effect of zeolite formation, facilitating the trapping of nuclear fission products.

CONCLUSIONS

The experimental results reveal a significant influence of the chemical composition of smectites on their reactivity in an alkaline environment at pH~13 and room *T*. The mineralogical evolution of montmorillonite and saponite follows a very distinct pathway under identical conditions. Extensive zeolite formation from montmorillonite will result in a reduction in the swelling capacity of a clay and, thus, in an improvement in water resistance of alkaline-treated earthen architecture. Under repository conditions, however, reduced swelling capacity will influence the sealing properties of the clay negatively, rendering it more permeable. The minor mineralogical changes in saponite suggest that water resistance or mechanical properties of earthen architecture containing trioctahedral smectites will not be improved significantly upon alkaline treatment. Under repository conditions, mineralogical changes are not desirable because they can cause a decrease in the swelling and sorption capacity of the clay, thereby increasing the permeability of the sealing material and rendering it ineffective. Thus, under these circumstances saponite can be considered as a viable candidate for use as a sealing material in nuclear-waste repositories, taking into account its long-term persistence in high-pH environments. Further research including *in situ* testing of both di- and trioctahedral smectitic clay barriers under repository conditions is warranted, however.

ACKNOWLEDGMENTS

The present study was supported financially by the Spanish Government (Grant CGL2012-35992) and the Junta de Andalucía (Research Group RNM-179). Special thanks to the Centro de Instrumentación Científica (University of Granada), in particular Dr Maria del Mar Abad Ortega, for assistance with FESEM, TEM, and elemental analyses, as well as the Instituto de Restauración y Conservación de Bienes Culturales (ICON, Fundación CICOP) for collaboration with this research project. The authors are indebted to Dr Fernando Nieto Garcia (Dept. of Mineralogy and Petrology, University of Granada) for assistance with the TEM and XRD analysis of clay minerals and for insightful comments on the manuscript.

REFERENCES

Barrer, R.M. (1982) *Hydrothermal Chemistry of Zeolites*, Academic Press, London, 360 pp.

Barrer, R.M., Cole, J.F., and Sticher, H. (1968) Chemistry of soil minerals. Part V. Low temperature hydrothermal transformations of kaolinite. *Journal of the Chemical Society (A)*, 2475–2485.

Barth-Wirsching, U. and Höller, H. (1989) Experimental studies on zeolite formation conditions. *European Journal of Mineralogy*, **1**, 489–509.

Bauer, A. and Velde, B. (1999) Smectite transformation in high molar KOH solutions. *Clay Minerals*, **34**, 259–273.

Bauer, A., Velde, B., and Berger, G. (1998) Kaolinite transformation in high molar KOH solutions. *Applied Geochemistry*, **13**, 619–629.

Beaufort, D. and Meunier, A. (1994) Saponite, corrensite and chlorite-saponite mixed-layers in Sancerre-Couy deep drill-hole (France). *Clay Minerals*, **29**, 47–61.

Beaufort, D., Baronnet, A., Lanson, B., and Meunier, A. (1997) Corrensite: A single phase or a mixed-layer phyllosilicate in the saponite-to-chlorite conversion series? A case study of Sancerre-Couy deep drill hole (France). *American Mineralogist*, **82**, 109–124.

Becerro, A., Mantovani, M., and Escudero, A. (2009) Mineralogical stability of phyllosilicates in hyperalkaline fluids: Influence of layer nature, octahedral occupation and presence of tetrahedral Al. *American Mineralogist*, **94**, 1187–1197.

Brady, P.V. and Walther, J.V. (1989) Controls on silicate dissolution rates in neutral and basic pH solutions at 25ºC. *Geochimica et Cosmochimica Acta*, **53**, 2823–2830.

Breck, D.W. (1974) *Zeolite Molecular Sieves – Structure, Chemistry and Use*. John Wiley & Sons, Inc., New York, 771 pp.

Brigatti, M.F. and Poppi, L. (1984) Crystal chemistry of corrensite: A review. *Clays and Clay Minerals*, **32**, 391–399.

Bristow, T.F., Kennedy, M.J., Derkowski, A., Droser, M.L., Jiang, G., and Creaser, R.A. (2009) Mineralogical constraints on the paleoenvironments of the Ediacaran Doushantuo Formation. *Proceedings of the National Academy of Sciences USA*, **106**, 13190–13195.

Brunauer, S., Emmett, P.H., and Teller, E. (1938) Adsorption of gases in multimolecular layers. *Journal of the American Chemical Society*, **60**, 309–319.

Csicsery, S.M. (1984) Shape-selective catalysis in zeolites. *Zeolites*, **4**, 202–312.

Cuadros, J. (2008) Clay as sealing material in nuclear waste repositories. *Geology Today*, **24**, 99–103.

Cuevas Rodriguez, J. (1993) Comportamiento hidrotermal de las arcillas saponiticas de la cuenca de Madrid. *Estudios Geológicos*, **49**, 137–146.

Cuevas, J., Pelayo, M., Rivas, P., and Leguey, S. (1993) Characterization of Mg-clays from the Neogene of the Madrid Basin and their potential as backfill and sealing material in high level radioactive waste disposal. *Applied Clay Science*, **7**, 383–406.

Cuevas, J., Garralon, A., Ramirez, S., and Leguey, S. (2001) Hydrothermal alteration of a saponitic bentonite: Mineral reactivity and evolution of surface properties. *Clay Minerals*, **36**, 61–74.

Davis, M.E. and Lobo, R.F. (1992) Zeolite and molecular sieve synthesis. *Chemistry of Materials*, **4**, 756–768.

Doehne, E. and Price, C.A. (2010) *Stone Conservation – An overview of current research*. The Getty Conservation Institute, Los Angeles, USA, 158 pp.

Drief, A., Nieto, F., and Sanchez-Navas, A. (2001) Experimental clay-mineral formation from a subvolcanic rock by interaction with 1 M NaOH solution at room temperature. *Clays and Clay Minerals*, **49**, 92–106.

Drief, A., Martinez-Ruiz, F., Nieto, F., and Velilla Sanchez, N. (2002) Transmission Electron Microscopy evidence for experimental illitization of smectite in K-enriched seawater solution at 50ºC and basic pH. *Clays and Clay Minerals*, **50**, 746–756.

Eberl, D.D., Velde, B., and McCormick, T. (1993) Synthesis of illite-smectite from smectite at earth surface temperature and high pH. *Clay Minerals*, **28**, 49–60.

Elert, K., Sebastian Pardo, E., and Rodriguez-Navarro, C. (2015) Alkaline treatment as an alternative method for the consolidation of earthen architecture. *Journal of Cultural Heritage*, **16**, 461–469.

Felsche, J., Luger, S., and Baerlocher, Ch. (1986) Crystal structures of the hydro-sodalite $Na_6[ALSiO_4]_6 \cdot 8H_2O$ and of the anhydrous sodalite $Na_6[ALSiO_4]_6$. *Zeolites*, **6**, 367–372.

Fernandez, R., Ruiz, A.I., and Cuevas, J. (2014) The role of smectite composition on the hyperalkaline alteration of bentonite. *Applied Clay Science*, **95**, 83–94.

Gaucher, E.C. and Blanc, P. (2006) Cement/clay interactions – a review: Experiments, natural analogues, and modeling. *Waste Management*, **26**, 776–788.

Gottardi, G. (1989) The genesis of zeolites. *European Journal of Mineralogy*, **1**, 479–487.

Groen, J.C., Pfeffer, L.A.A., and Perez-Ramirez, J. (2003) Pore size determination in modified micro- and mesoporous materials. Pitfalls and limitations in gas adsorption data analysis. *Microporous and Mesoporous Materials*, **60**, 1–17.

Hauff, P. (1981) *Corrensite: Mineralogical Ambiguities and Geologic Significance*. Geological Survey, Open-File Report 81-850, US Department of the Interior, 45 pp.

Hensen, E.J.M. and Smit, B. (2002) Why clays swell. *Journal of Physical Chemistry B*, **106**, 12664–12667.

Huertas, F.J., Carretero, P., Delgado, J., Linares, J., and Samper, J. (2001) An experimental study on the ion-exchange behaviour of the smectite of Cabo de Gata (Almeria, Spain): FEBEX bentonite. *Journal of Colloid and Interface Science*, **239**, 409–416.

Karamalidis, A.K. and Dzombak, D.A. (2010) *Surface Complexation Modeling: Gibbsite*. John Wiley & Sons, Inc., New Jersey, 294 pp.

Karnland, O., Olsson, S., Nilsson, U., and Sellin, P. (2007) Experimentally determined swelling pressures and geochemical interactions of compacted Wyoming bentonite with highly alkaline solutions. *Physics and Chemistry of the Earth*, **32**, 275–286.

Kirov, G. and Filizova, L. (2012) Cationic hydration impact on zeolite formation and properties: A review and discussion. *Geochemistry, Mineralogy and Petrology – Sofia*, **49**, 65–82.

Kovalchuk, G., Fernandez-Jimenez, A., and Palomo, A. (2008) Activacion alcalina de cenizas volantes. Relación entre el desarrollo mecánico resistente y la composición química de la ceniza. *Materiales de Construcción*, **58**, 35–52.

Li, D., Yao, J., Wang, H., Hao, N., Zhao, D., Ratinac, K.R., and Ringer, S.P. (2007) Organic-functionalized sodalite nanocrystals and their dispersion in solvents. *Microporous and Mesoporous Materials*, **106**, 262–267.

Lorimer, G.W. and Cliff, G. (1976) Analytical electron microscopy of minerals. Pp. 506–519 in: *Electron Microscopy in Mineralogy* (H.R. Wenk, editor). Springer-Verlag, New York.

Meunier, A., Velde, B., and Griffault, L. (1998) The reactivity of bentonites: a review. An application to clay barrier stability for nuclear waste storage. *Clay Minerals*, **33**, 187–196.

Miyaji, F., Murakami, T., and Suyama, Y. (2009) Formation of linde F by KOH treatment of coal fly ash. *Journal of the Ceramic Society of Japan*, **117**, 619–622.

Moliner, M. (2012) Direct synthesis of functional zeolitic materials. *International Scholarly Research Network Materials Science*, 24 pp.

Mosser-Ruck, R. and Chathelineau, M. (2004) Experimental transformation of Na,Ca-smectite under basic conditions at 150ºC. *Applied Clay Science*, **26**, 259–273.

Mumpton, F.A. (1985) Using zeolites in agriculture. Pp. 127–157 in: *Innovative Biological Technologies for Lesser Developed Countries*. Congress of the US, Office of Technology Assessment, Washington D.C.

Murakami, T., Sato, T., and Inoue, A. (1999) HRTEM evidence for the process and mechanism of saponite-to-chlorite conversion through corrensite. *American Mineralogist*, **84**, 1080–1087.

Nagy, K.L. (1995) Dissolution and precipitation kinetics of sheet silicates. Pp. 173–225 in: *Chemical Weathering Rates of Silicate Minerals* (A.F. White and S.L. Brantley, editors). Reviews in Mineralogy, **31**, Mineralogical Society of America, Washington D.C.

Newman, A.C.D. and Brown, G. (1987) The chemical constitution of clay. Pp. 1–128 in: *Chemistry of Clays and Clay Minerals* (A.C.D. Newman, editor). Mineralogical Society Monograph, **6**, Longman Scientific & Technical, London.

Norrish, K. (1954) The swelling of montmorillonite. *Discussions of the Faraday Society*, **18**, 120–134.

Pokrovsky, O.S. and Schott, J. (2004) Experimental study of brucite dissolution and precipitation in aqueous solution: Surface speciation and chemical affinity control. *Geochimica et Cosmochimica Acta*, **68**, 31–45.

Pozo Rodríguez, M. and Casas Sainz de Aja, J. (1992) Mineralogía y sedimentología del yacimiento de saponita de Yuncos (Toledo). *Estudios Geologicos*, **48**, 47–65.

Prieto, O., Vicente, M.A., and Bañares-Muñoz, A. (1999) Study of the porous solids obtained by acid treatment of a high surface area saponite. *Journal of Porous Materials*, **6**, 335–334.

Ramirez, S., Cuevas, J., Vigil, R., and Leguey, S. (2002) Hydrothermal alteration of "La Serrata" bentonite (Almeria, Spain) by alkaline solutions. *Applied Clay Science*, **21**, 257–269.

Rouquerol, J., Rouquerol, F., and Sing, K.S.W. (1998) *Absorption by Powders and Porous Solids*. Academic Press, San Diego, 467 pp.

Roy, D.M. (1999) Alkali-activated cements. Opportunities and challenges. *Cement and Concrete Research*, **29**, 249–254.

Rozalen, M., Brady, P.V., and Huertas, F.J. (2009) Surface chemistry of K-montmorillonite: Ionic strength, temperature dependence and dissolution kinetics. *Journal of Colloid and Interface Science*, **333**, 474–484.

Sanchez, L., Cuevas, J., Ramirez, S., Ruiz de Leon, D., Fernandez, R., Vigil dela Villa, R., and Leguey, S. (2006) Reaction kinetics of FEBEX bentonite in hyperalkaline conditions resembling the cement-bentonite interface. *Applied Clay Science*, **33**, 125–141.

Siegel, M.D., Leckie, J.O., Park, S.W., Phillips, S.L., and Sewards, T. (1990) Studies of radionuclide sorption by clays in the Culebra dolomite at the Wipp site, southeastern New Mexico. Pp. 839–900 in: *Technical Report SAND-89-2387*, Sandia National Labs, Albuquerque, NM (USA).

Sing, K.S.W., Everett, D.H., Haul, R.A.W., Moscou, L., Pierotti, R.A., Rouquerol, J., and Siemieniewska, T. (1985) Reporting physisorption data for gas/solid systems. *Pure and Applied Chemistry*, **57**, 603–619.

Singh, R. and Dutta, P.K. (1998) Stabilization of natural faujasite zeolite: possible role of alkaline earth metal ions. *Microporous and Mesoporous Materials*, **21**, 103–109.

Slaty, F., Khoury, H., Wastiels, J., and Rahier, H. (2013) Characterization of alkali activated kaolinitic clay. *Applied Clay Science*, **75–76**, 120–125.

Somasundaran, P. and Agar, G.E. (1967) The zero point of charge of calcite. *Journal of Colloid and Interface Science*, **24**, 400–433.

Sposito, G. (1984) *The Surface Chemistry of Soils*. Oxford University Press, New York, 234 pp.

Stumm, W. (1997) Reactivity at the mineral–water interface: Dissolution and inhibition. *Colloids and Surfaces A*, **120**, 143–166.

Suarez Barrios, M., Vicente-Rodriguez, M.A., and Martin Pozas, J.M. (1996) Intercalation compounds between nicotine and a high surface area saponite. *Journal of Inclusion Phenomena and Molecular Recognition in Chemistry*, **24**, 263–272.

Sutarno, S. and Arryanto, Y. (2007) Synthesis of faujasite from fly ash and its application for hydrocracking of petroleum distillates. *Bulletin of Chemical Reaction Engineering and Catalysis*, **2**, 45–51.

Villar, M.V., Perez del Villar, L., Martin, P.L., Pelayo, M., Fernandez, A.M., Garralon, A., Cuevas, J., Leguey, S., Caballero, E., Huertas, F.J., Jimenez de Cisneros, C., Linares, J., Reyes, E., Delgado, A., Fernandez-Soler, J.M., and Astudillo, J. (2006) The study of Spanish clays for their use as sealing materials in nuclear waste repositories: 20 years of progress. *Journal of Iberian Geology*, **32**, 15–36.

Whitney, D.L. and Evans, B.W. (2010) Abbreviations for names of rock-forming minerals. *American Mineralogist*, **95**, 185–187,

(*Received 9 April 2015; revised 15 January 2016; Ms. 990; AE: R.J. Pruett*)